results indicated that reduced VEGF levels in NP–C PNs caused a defect of autophagic degradation, but not induction.

Our findings that depletion of VEGF affects autophagic degradation prompted us to more closely examine how VEGF might influence in defective autophagic degradation. We first examined the transcription factor EB (TFEB), which coordinates lysosomal formation[24]. VEGF depletion in WT PNs did not affect the levels of TFEB and Lamp1, indicating that VEGF did not impair lysosome biogenesis (Fig. 6e). Next, we assessed alteration in lysosomal pH using the acidotropic dye LysoTracker red. H_2O_2- and NH_4Cl-treated cells were used as positive and negative controls, respectively. VEGF siRNA-treated PNs exhibited a similar fluorescence to control siRNA-treated PNs, indicating that VEGF did not affect lysosomal acidification (Fig. 6f).

Following the initiation of the phagophores, autophagosomes undergo a stepwise maturation process from early to late autophagosomes, which ultimately fuse with lysosomes to form autolysosomes. To study the effect of VEGF depletion on the maturation of autophagosomes, we used mCherry-EGFP-LC3 reporter[25]. Before fusion with lysosomes, the LC3-II-positive autophagosomes are shown by both GFP and mCherry signals as yellow puncta, and after fusion, autolysosomes are shown by only mCherry signals as red-only puncta because GFP loses its fluorescence in acidic pH. Compared with control PNs, VEGF siRNA-treated cells showed significantly increased yellow puncta (autophagosomes) and decreased mCherry-only puncta (autolysosomes), indicating that VEGF depletion inhibited the autophagosome–lysosome fusion (Fig. 6g).

Sphingosine accumulation can induce defective calcium release from the acidic compartment such as lysosome, which inhibits fusion of lysosome with other organelles[4]. As shown in Supplementary Figs 2g and 3h, decreased VEGF levels caused sphingosine accumulation in WT PNs. Thus, we hypothesized that defective lysosomal calcium release by VEGF-mediated sphingosine accumulation disturbs autophagosome–lysosome fusion and evokes the abnormal autophagosomes' amassment. To test this hypothesis, we used the weaker sarcoplasmic reticulum ATPase antagonist curcumin, a natural product derived from turmeric[26], which correct sphingolipid imbalance by increasing the cytosolic calcium release[4]. Importantly, abnormal sphingolipid levels in the VEGF siRNA-treated PNs were normalized after curcumin treatment (Fig. 6h). We also observed significantly decreased protein level of abnormal autophagic markers (Fig. 6i) and increased neuronal survival (Fig. 6j) in the VEGF-knockdown PNs after curcumin treatment compared with PNs with VEGF knockdown alone. Similar results were observed in the VEGF shRNA-treated mice after curcumin injection (Supplementary Fig. 6). To further examine these effects, we analysed calcium homeostasis in the primary cultured PNs derived from WT, NP–C and VEGF/NP–C mice. To specifically assess the lysosomal calcium content, we used Gly–Phe β-naphthylamide (GPN), which osmotically lyses cathepsin-containing lysosome[4]. We observed a reduction in NP–C PNs' calcium release from lysosome compared with WT PNs, consistent with our previous study[7]. Notably, this reduction was corrected in VEGF/NP–C PNs (Fig. 6k). As expected, abnormal sphingosine accumulation was reduced in VEGF/NP–C cells by restoration of SphK activity (Fig. 6l). Moreover, VEGF/NP–C PNs showed decreased autophagosome (yellow LC3 puncta) accumulation (Fig. 6m). Decreased autophagosomes in the VEGF/NP–C PNs were further confirmed by EM analysis (Fig. 6n). The survival of PNs was also significantly increased in the VEGF/NP–C (Fig. 6o). Together, these findings show that inactivated VEGF/SphK pathway in NP–C PNs causes sphingosine accumulation and this amassment inhibits autophagosome–lysosome fusion by disturbance of calcium homeostasis.

VEGF rescues autophagic defects in patient-specific cells. To further validate our observation regarding VEGF treatment in NP–C mice, we studied effects of VEGF on SphK activity in human NP–C fibroblasts. Human NP–C fibroblasts cocultured with human BM-MSCs, $VEGF^{tg}$ BM-MSCs or treated with recombinant VEGF showed significantly increased SphK activity, decreased sphingosine and elevated S1P (Supplementary Fig. 7a–c). Increased LC3-II levels and p62 accumulation in NP–C fibroblasts were reduced by VEGF treatment (Supplementary Fig. 7d,e). VEGF-treated NP–C fibroblasts also showed increased calcium release and decreased autophagosome accumulation (as judged by yellow LC3 puncta) compared with non-treated NP–C fibroblasts (Supplementary Fig. 7f,g). Lysosomal exocytosis is necessary to affect clearance of stored intracellular lipids and ameliorates the endolysosomal lipid storage phenotype in NP–C cells[27]. To determine whether VEGF directly induced lysosomal exocytosis, the culture media of normal and NP–C fibroblasts treated with or without VEGF were analysed for the presence of the lysosomal enzyme β-hexosaminidase as a marker for lysosomal content secretion. In all groups, the activity of β-hexosaminidase was not significantly elevated at the indicated times (Supplementary Fig. 7h). The low-level appearance of β-hexosaminidase in the culture media of fibroblasts is not a result of generalized cell lysis, since the levels of lactate dehydrogenase (LDH) in the media remained unchanged in all groups for the duration of the assay (Supplementary Fig. 7h). These results suggested that the ability of

Figure 7 | VEGF ameliorates sphingolipid imbalance in NP-C iPSC neurons. (**a**) Left, normal, hNPC-3 and hNPC-17 iPSCs generated nestin-positive neuroprogenitor cells (scale bar, 50 μm). Right, representative images of immunocytochemical staining the β-III tubulin following neural differentiation (scale bar, 50 μm). (**b**) hNPC-3 and hNPC-17 neurons were treated with human BM-MSCs, $VEGF^{tg}$ BM-MSCs or recombinant VEGF (10 ng ml^{-1}). Three days after treatment, VEGF levels were measured in cell lysates. (**c–f**) SphK activity (**c**), sphingosine (**d**), S1P (**e**) and sphingomyelin (**f**) were measured in normal iPSC neurons and hNPC neurons with or without treatment. (**g**) Filipin staining of unesterified cholesterol in hNPC-3 neurons with or without treatment of recombinant VEGF for 3 days (scale bar, 50 μm). Quantification of filipin fluorescence intensities normalized to normal neurons. Unesterified cholesterol levels in normal iPSC neurons and hNPC neurons with or without treatment were measured ($n=6$ per group). (**h**) Effect of the VEGFR2 inhibitor on VEGF mediated sphingolipid modulation. hNPC-3 neurons were pretreated with PTK787 at 10 μM for 1 day and were treated for 3 days with 10 ng ml^{-1} VEGF and then assayed for SphK activity, sphingosine and S1P ($n=7$ per group). (**i,j**) Effect of NPC1 knockdown on sphingolipid factors in normal iPSC neurons. (**i**) Three days after NPC1 siRNA transfection, we measured the levels of *NPC1* mRNA and VEGF expression. (**j**) SphK activity, sphingosine and S1P were measured in normal iPSC neurons treated with control or NPC1 siRNA (control, $n=7$; NPC1 siRNA, $n=9$). (**k**) Effect of VEGF knockdown on sphingolipid factors in normal iPSC neurons. Three days after VEGF siRNA transfection, we measured the levels of *VEGF* mRNA, SphK activity, sphingosine and S1P in normal iPSC neurons ($n=7$ per group). (**l**) Effect of a specific SphK1 inhibitor on sphingolipid factors in normal iPSC neurons. Normal neurons were treated with or without 20 μM SK1-I for 6 h. Lipids were extracted and sphingosine, S1P and unesterified cholesterol levels were determined ($n=6$ per group). **b–h**, one-way analysis of variance, Tukey's *post hoc* test. **i–l**, Student's *t*-test. $^*P<0.05$, $^{**}P<0.01$, $^{***}P<0.005$. All error bars indicate s.e.m.

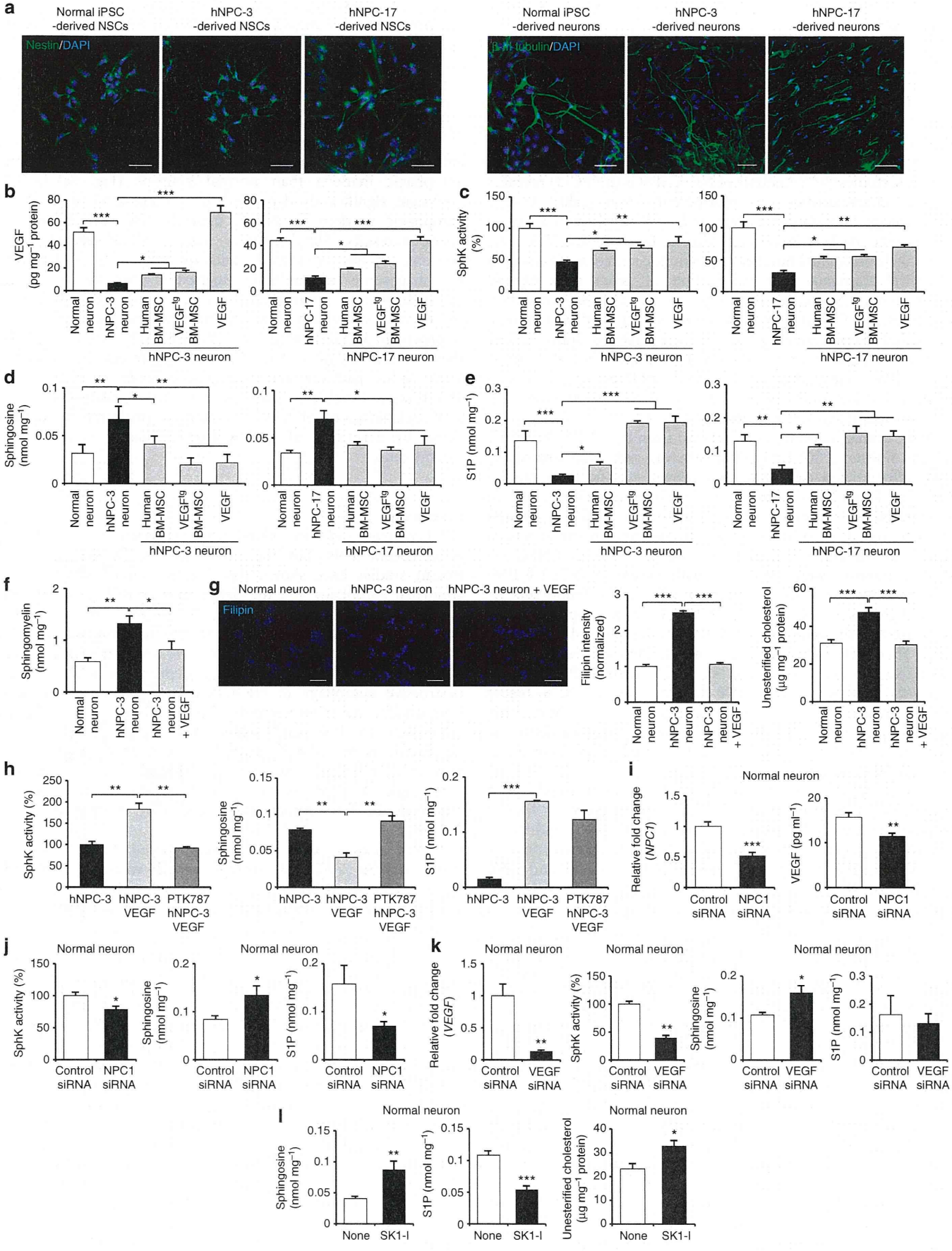

VEGF to reduce sphingosine storage in NP-C cells was not due to lysosomal exocytosis.

The recent developments in induced pluripotent stem cells (iPSCs) and iPSC-derived neurons have allowed investigation of pathogenesis of neurological diseases *in vitro*. To explore whether the observed effects of VEGF we describe above were similar in NP-C human neurons, we established human NP-C iPSCs (hNPC-3, 6, 17) by transduction of human NP-C fibroblasts with retroviruses encoding *OCT4*, *SOX2*, *KLF4* and *c-MYC* similar to previous studies[28–30]. Analysis of NP-C iPSCs (hNPC-3) revealed typical characteristics of pluripotent stem cells: similar morphology to embryonic stem cells (ES cells), expression of pluripotent markers including SSEA-4, Tra-1-60 and Tra-1-81, normal chromosomal number and genomic structure, silencing of retroviral transgene and reactivation of genes indicative of pluripotency (Supplementary Fig. 8a–c). The differentiation ability of NP-C iPSCs was also confirmed *in vivo* by teratoma formation (Supplementary Fig. 8d). We analysed SphK activity and sphingolipid levels in the normal iPSC and NP-C iPSC lines. NP-C iPSC lines exhibited decreased SphK activity, increased sphingosine accumulation and decreased S1P levels compared with normal iPSCs (Supplementary Fig. 8e).

Next, human neurons were induced from the hNPC-3, hNPC-17 and normal iPSC. Early-differentiating cells expressed nestin and differentiated cells expressed neuron-specific β-III tubulin (Fig. 7a). These NP-C neurons also exhibited phenotypes seen in human NP-C samples, including abnormal VEGF levels and sphingolipid metabolism (Fig. 7b–e). To confirm the effects of VEGF in human NP-C neurons, the hNPC-3- or hNPC-17-derived neurons were cocultured with human or $VEGF^{tg}$ BM-MSCs, or treated with recombinant VEGF. We found that all treated groups exhibited increased VEGF, elevated SphK activity, decreased sphingosine accumulation and increased S1P levels (Fig. 7b–e). Sphingomyelin and unesterified cholesterol levels were also significantly decreased in VEGF-treated NP-C neurons (Fig. 7f,g). We also pretreated NP-C neurons with PTK787 before VEGF treatment. We found that SphK activity and other sphingolipid metabolites in NP-C neurons were mediated by interactions of VEGF and its receptor VEGFR2 in these iPSC-derived NP-C neurons (Fig. 7h).

To reconfirm the *in vitro* mechanism whereby there is a direct relationship between *NPC1*, VEGF and SphK activity in human neurons, we treated normal iPSC neurons with NPC1 and VEGF siRNA (Fig. 7i–k) and determined changes in various sphingolipid factors. NPC1 siRNA decreased VEGF expression and SphK activity (Fig. 7i,j). VEGF siRNA also strongly inactivated SphK levels (Fig. 7k). Both siRNA treatments led to changed levels of sphingosine and S1P, similar to NP-C neurons (Fig. 7j,k). To determine whether reduction in SphK activity affected sphingolipid factors and unesterified cholesterol in iPSC neurons similar to those in classical NP-C cells, we treated the normal iPSC neurons with a specific SphK1 inhibitor, SK1-I. We found that inhibition of SphK activity increased sphingosine and unesterified cholesterol accumulation and decreased cellular S1P (Fig. 7l).

We also examined whether NP-C neurons exhibited abnormal autophagy. NP-C neurons had significantly higher abnormal autophagic markers than normal neurons (Fig. 8a). VEGF treatment significantly decreased the protein level of abnormal autophagic markers in NP-C neurons (Fig. 8a). Similar to previous results (Supplementary Fig. 7), VEGF-treated NP-C neurons showed increased calcium release and decreased autophagosome accumulation, suggesting that VEGF elevates autophagosome–lysosome fusion (Fig. 8b–d). Consistent with the restored autophagy flux, cell survival was also significantly improved in VEGF-treated NP-C neurons (Fig. 8e). Collectively, these results confirm that defective autophagy by abnormal VEGF/SphK pathway and sphingosine levels in NP-C mice and human fibroblasts also occur in NP-C patient neurons, and replenishment of VEGF is able to ameliorate autophagy defect by correction of sphingolipid imbalance in the NP-C patient cells.

Discussion

NP-C patients and mice exhibit progressive neuronal loss, mainly of cerebellar PNs, but the mechanism is largely unknown. Recent studies have shown that inactivation of NPC1 caused abnormal autophagy and the defect may contribute to PN loss in NP-C[22]. Loss of NPC1 function leads to trapping of lipids within aberrant membrane compartments, and this may induce a 'lipid-starvation response' analogous to the well-characterized autophagic response to amino-acid deprivation[31]. In addition, destructive autophagy in NP-C PNs may also be stimulated hormonally via neurosteroids. Neurosteroids might inhibit autophagy in PNs and when their synthesis is severely decreased, as in NP-C[32], autophagic cell death might ensue. Similar to previous results[22,33], we found that the impaired autophagic flux in NP-C was associated with decreased autophagosome–lysosome fusion, and that this defect led to PNs loss.

Recent studies have also demonstrated that cholesterol, sphingomyelin and GSL storage are downstream events in NP-C disease pathogenesis caused by sphingosine storage, leading to altered acidic compartment calcium levels[4]. They

Figure 8 | VEGF rescues the autophagic defects in NP-C iPSC neurons. (**a**) Western blot analysis of LC3 and p62 in normal and NP-C iPSC-derived neurons treated with or without 10 ng ml^{-1} recombinant VEGF (normal, $n=6$; hNPC, $n=7$; and VEGF-treated hNPC, $n=7$). (**b**) Left, representative traces showing intracellular [Ca^{2+}] changes monitored in single fluo-4-loaded normal and NP-C iPSC neurons treated with or without recombinant VEGF (10 ng ml^{-1}). Right, maximal peak fluorescence changes were determined as the differences between basal and the maximum fluorescence, on addition of 200 μM GPN ($n=10$ cells per group). (**c**) Fluorescence staining and quantification of autophagosomes (mCherry^{+}-EGFP^{+}-LC3) and autolysosomes (mCherry^{+}-EGFP^{-}-LC3) in normal and NP-C iPSC neurons after recombinant VEGF treatment (normal, $n=7$; hNPC, $n=8$; and VEGF-treated hNPC, $n=8$; scale bar, 10 μm). (**d**) EM images and quantification data of normal and NP-C iPSC-derived neurons after 10 ng ml^{-1} VEGF treatment ($n=5$ per group; low-magnification scale bar, 1 μm; high-magnification scale bar, 200 nm). (**e**) Quantification of cell viability (normal, $n=5$; hNPC, $n=6$; and VEGF-treated hNPC, $n=6$). (**f**) Model of VEGF-mediated SphK activation in NP-C neurons. (A,B) In NP-C cells, sphingosine accumulation is increased due to defective SphK activity together with decreased VEGF caused by mutated NPC1 and defective uptake via VEGFR2. (C) Abnormal sphingosine accumulation decreases calcium release from lysosomes and the reduction in calcium release causes an autophagic defect by inhibiting autophagosome-lysosome fusion. Eventually, these defects cause loss of cerebellar neurons. (D,E) When NP-C neurons are exposed to BM-MSCs or pure VEGF, the cells exhibit elevated intracellular levels of VEGF (F), which induces VEGFR2-mediated activation of SphK in the cytosol and lysosome. (G) This activation leads to decreased sphingosine accumulation and increased S1P levels. (H) Reduced sphingosine accumulation results in improved autophagosome-lysosome fusion by correction of calcium homeostasis. Finally, this restoration prevents neuronal loss in NP-C. **a**–**e**, one-way analysis of variance, Tukey's *post hoc* test. *$P<0.05$, **$P<0.01$, ***$P<0.005$. All error bars indicate s.e.m.

have determined the chronology of events after inactivation of NPC1. In a drug-induced NP-C cellular model, sphingosine storage in the acidic compartment led to calcium depletion in these organelles, which then resulted in cholesterol, sphingomyelin and GSL storage in these compartments. Therefore, sphingosine storage might be an initiating factor in NPC1 disease pathogenesis that causes altered calcium homeostasis, leading to the secondary storage of sphingolipids and cholesterol, although additional studies are required. Similarly, we found that VEGF-mediated sphingosine modulation also significantly decreased sphingomyelin and unesterified cholesterol levels. Therefore, we suggest that

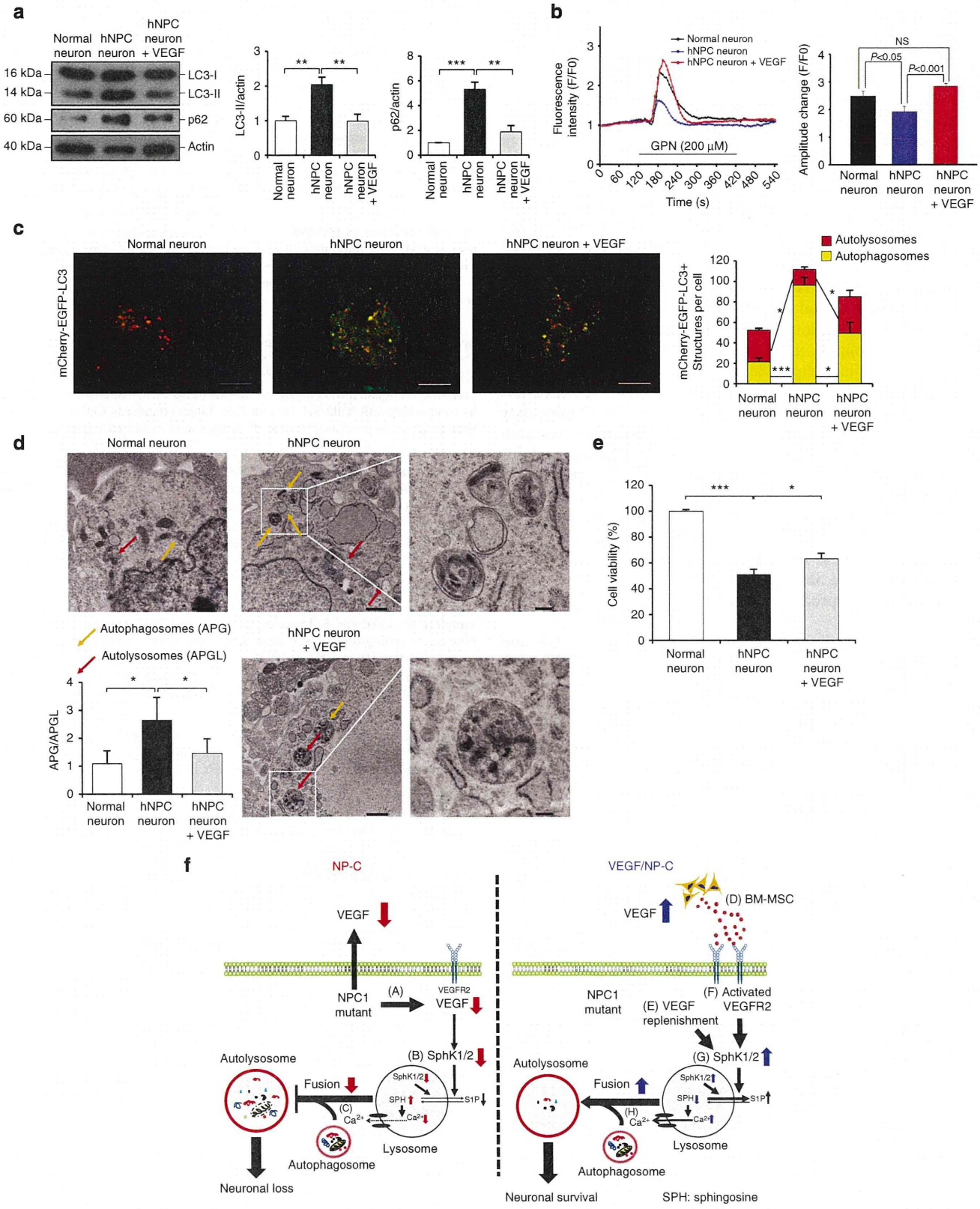

replenishment of VEGF is able to ameliorate accumulation of sphingomyelin and unesterified cholesterol by reducing sphingosine accumulation in the NP–C. Similar to sphingosine accumulation, cholesterol accumulation also induced changes in autophagy–lysosome function in PNs and lead to death of these cells. In NP–C mouse brain, combined LC3 immunofluorescence and filipin staining showed that LC3 accumulated within filipin-labelled cholesterol clusters inside PNs[34]. These results provide strong evidence that cholesterol accumulation-induced changes in autophagy–lysosome function are closely associated with neurodegeneration in NP–C. Therefore, we suggest that reduced PN survival in NP–C may be due to impaired autophagic flux by VEGF/SphK pathway-mediated sphingosine accumulation and secondary storage of cholesterol.

Despite extensive data supporting the modulating effect of VEGF on SphK in NP–C, the clinical effectiveness of VEGF-mediated therapy in the NP–C mouse model was the modest. There are several potential explanations for this finding. First, it must be recognized that in these animal model experiments the primary lesion in the *Npc1* gene and protein remains in the treated mice, and thus correction of their sphingolipid imbalance via VEGF may only slow progression and require additional, combinational therapies to achieve a more complete clinical effect. In addition, VEGF may not be the only factor regulating sphingolipid metabolism in NP–C, as suggested by the fact that the sphingolipid levels were improved, but not normalized, in the treated cells and mice. Finally, the methods used to introduce VEGF into the brain of the NP–C mice may need to be improved, and there are considerable research underway exploring different approaches to introducing proteins such as VEGF into the central nervous system[35,36]. Indeed, small molecules may also be developed in the future that modulate VEGFR2 leading to SphK enhancement, or even small molecules that work on SphK directly. Despite the limitations of these animal model studies, however, the findings reported in the manuscript describe a novel pathogenic mechanism in NP–C and reveal a potential approach for the therapy via the VEGF/SphK pathway.

In summary, the data presented here show that VEGF and SphK activities are reduced in both NP–C mouse PNs and patient-specific cells, and that correction of this activity by VEGF (released from BM-MSCs or added directly into the CNS) can reduce NP–C pathological changes via increasing autophagic degradation (Fig. 8f). Thus, VEGF is a therapeutic candidate for NP–C that influences sphingosine storage via SphK modulation, suggesting that enhancing SphK activity is a potential therapeutic intervention for this disorder.

Methods

Mice. A colony of Balb/c *Npc1*^{nih} mice has been maintained and the genotype of each mouse was determined by PCR using forward (5′-GGTGCTGGACAGCCA AGTA-3′) and reverse primer (5′-GATGGTCTGTTCTCCCATG-3′)[37]. VEGF-overexpressing transgenic mice[14] were bred with NP–C mice to generate VEGF/NP–C (*VEGF*^{tg}/*Npc1*$^{-/-}$) mice. Four-week-old mice were used for transplantation of BM-MSCs and microspheres. We choose the block randomization method to allocate the animals to experimental groups. For the cerebellar transplantation[7], the injections were carried out using a glass capillary (1.2 × 0.6 mm). The injection coordinates were 5.52 mm posterior to bregma and injection depth was 2.50 mm. In some experiments, mice were treated with the VEGFR inhibitor PTK787/ZK222584 (PTK787; 100 mg kg^{-1}, Selleck Chemicals) or PBS vehicle control by oral gavage once a day for 3 days. PTK787 is a potent and relatively selective inhibitor of all VEGF receptor tyrosine kinases, with greater activity against VEGFR2[17]. Three-week-old WT mice were treated with VEGF shRNA and curcumin (Supplementary Fig. 6a). Eight-week-old male SCID Beige mice (Charles River Laboratories) were used for teratoma formation assay. To eliminate the bias, we were blinded in experimental progress such as data collection and data analysis. Mice were housed at a 12 h day–night cycle with free access to tap water and food pellets. Mouse studies were approved by the Kyungpook National University Institutional Animal Care and Use Committee.

Cell isolation and culture. Human *NPC1*-mutant and control fibroblasts (GM03123 and GM05399, respectively) were acquired from the Coriell Institute and were used at passages 10–15. Primary PN cultures were prepared from the cerebellum of individual embryonic day 18 fetuses[7]. The cerebellum was dissociated using the Nerve-Cell Culture System (Sumitomo Bakelite) and plated in the PN culture media[7]. To isolate mouse BM-MSCs[6], bone marrow was harvested from tibias and femurs of 4- to 6-week-old Balb/c or VEGF-overexpressing transgenic mice, and single-cell suspensions were obtained using a 40-μm cell strainer (BD Biosciences). Cells containing MesenCult MSC Basal Medium plus Supplements (Stemcell Technologies) were plated. Normal iPSC line (HPS0063) was obtained from the RIKEN Bioresource Center[38]. Human BM-MSCs were kindly provided by the Cell Therapy Center of Yonsei University. Informed consent was obtained from all subjects according to the ethics committee guidelines at the Yonsei University Severance Hospital. For some experiments, cells were treated with human recombinant VEGF (R&D Systems), human and mouse SMART pool VEGF siRNA (Dharmacon), human and mouse SMART pool NPC1 siRNA (Dharmacon) or scrambled sequence siRNA control (Dharmacon). NH_4Cl was used to inhibit autophagic flux. Curcumin (Sigma-Aldrich) was used to increase cytosolic calcium release. For the inhibition of VEGFR2 signal activation *in vitro*, cells were pretreated for 1 day with 10 μM of PTK787. For the inhibition of SphK1 activation *in vitro*, cells were pretreated for 6 h with 20 μM of SK1-I (Enzo Life Sciences).

Indirect coculture of BM-MSCs. For the indirect coculture experiments, 1.0 μm pore size Millicell Hanging Cell Culture Inserts (Millipore) were placed on top of the previously plated cells. BM-MSCs were seeded onto the insert at a density of 3×10^4 cells per insert. In this system there was no direct contact between cocultured cells and BM-MSCs.

SphK activity assays. SphK activity was followed as phosphorylation of (7-nitro-2-1,3-benzoxadiazol-4-yl)-d-erythro (NBD)-sphingosine (Avanti Polar Lipids) to NBD-S1P as described previously[39] with modification using a UPLC (ultra performance liquid chromatography) system (Waters). Quantification was achieved by comparison with NBD-S1P (Avanti Polar Lipids) standards. Cell and tissue lysates were prepared as previously described[7]. Values were expressed as percent of control.

Lipid extraction and sphingosine/S1P/sphingomyelin quantification. Samples were lysed in homogenization buffer containing 50 mM HEPES (Gibco), 150 mM NaCl (Sigma-Aldrich), 0.2% Igepal (Sigma-Aldrich) and protease inhibitor (Calbiochem)[7]. To quantify the sphingosine, S1P and sphingomyelin levels, the dried lipid extract was resuspended in 0.2% Igepal CA-630. Four microlitres of the lipid extracts was added into 20 μl of NDA derivatization reaction mixture (25 mM borate buffer, pH 9.0, containing 2.5 mM each of NDA and NaCN). The reaction mixture was diluted 1:3 with ethanol, incubated at 50 °C for 10 min and centrifuged (13,000*g* for 5 min). An aliquot (30 μl) of the supernatant was then transferred to a sampling glass vial and 5 μl was applied onto an UPLC system for analysis. The fluorescent sphingosine or S1P derivatives were monitored using a model 474 scanning fluorescence detector (Waters). Quantification of the sphingosine, S1P and sphingomyelin peaks were calculated from sphingosine, S1P and sphingomyelin standard calibration curves using the Waters Millennium software.

Cytokine antibody array. RayBio Custom Mouse Cytokine Antibody Arrays (RayBiotech) were employed for assay of cell culture supernatants from coculture experiments according to the manufacturer's instructions.

ELISA. VEGF protein levels were assayed by using a Mouse and Human VEGF Quantikine kit (R&D Systems) according to manufacturer's instructions.

Immunofluorescence staining. For the immunofluorescence staining, cells and brain sections were blocked with PBS containing 5% normal goat serum (Vector Laboratories), 2% BSA (Gibco) and 0.4% Triton X-100 (Sigma-Aldrich). In the same buffer solution, the cells and sections were then incubated for 24 h with primary antibodies. The following antibodies were used: anti-VEGF (rabbit, 1:500, Invitrogen, ab39250), anti-calbindin (rabbit, 1:500, Chemicon, ab82812 and mouse, 1:500, Abcam, ab9481), anti-S1P (mouse, 1:400, Alfresa Pharma, 274594052), anti-LC-3B (rabbit, 1:200, Cell Signaling Technologies, 3868S), anti-active caspase-3 (rabbit, 1:50, Chemicon, AB3623), anti-β-III tubulin (mouse, 1:400, Chemicon, MAB1637), anti-nestin (mouse, 1:400, Chemicon, MAB353), anti-SSEA-4, TRA-1-60 and TRA-1-81 (mouse, 1:100, Chemicon, MAB4304, MAB4360 and MAB4381). The cells and sections were analysed with a laser scanning confocal microscope equipped with Fluoview SV1000 imaging software (Olympus FV1000) or with an Olympus BX51 microscope. Metamorph software (Molecular Devices) was used to calculate the average intensity.

Filipin staining. Cells and cerebellar sections were fixed with 4% paraformaldehyde for 15 min, washed with PBS and incubated for 30 min with 100 μg ml^{-1} filipin (Polysciences) in PBS. Cells and cerebellar sections were washed twice with PBS for 5 min. The averaged intensities were analysed as described above.

Amplex red assay. The cells and cerebellar tissues were lysed with lysis buffer (50 mM phosphate buffer, 500 mM NaCl, 25 mM cholic acid and 0.5% Triton X-100). The unesterified cholesterol was determined using the Amplex Red Cholesterol Assay Kit (Molecular Probes) according to the manufacturer's instructions. After incubation for 30 min at 37 °C, the fluorescence intensities were measured on a microplate reader (Molecular devices) equipped with a filter set for excitation and emission at 560 ± 10 nm and 590 ± 10 nm, respectively. The cholesterol content was calculated with a cholesterol standard curve. Cellular cholesterol content was normalized to protein content.

GSL analysis. Cerebellum from 6-week-old mice was homogenized with four volumes of ice-cold water in an all-glass Potter-Elvehjem homogenizer; 250 µl of homogenate (50 mg of wet tissue) was extracted by addition of 1.2 ml of methanol and 2 ml of chloroform. After incubation of the samples at 37 °C for 1 h, 1 ml of methanol was added, and the extracts were centrifuged at 2,000 *g* for 10 min. The pellet was re-extracted with 2 ml of chloroform/methanol/water (1/2/0.8, v/v/v) at 37 °C for 2 h. The combined supernatants were concentrated by Speed-Vac, and the dried samples were dissolved in 2 ml of methanol and saponified. After neutralization, samples were diluted with 2 ml of water and desalted using OASIS HLB 1 cc extraction cartridges (Waters). Thin-layer chromatography was performed using HPTLC (Merck) and developed with chloroform/methanol/0.02% $CaCl_2$ (5:4:1, v/v). After staining with orcinol–sulfuric acid, GSLs were identified by comparing their R_F to those of authentic GSL standards.

Isolation of cytosolic-enriched and lysosome-enriched fractions. Cerebellum from 6-week-old mice was washed twice with cold PBS, and then cytosolic-enriched and lysosome-enriched fractions were extracted. Lysosomes were isolated on sucrose gradient by using a lysosome isolation kit from Sigma-Aldrich. β-*N*-acetyl-glucosaminidase activity quantifications (Sigma-Aldrich), according to the manufacturer instructions, was used to identify lysosomal fractions. Cytosolic-enriched fractions (hydrophilic) were extracted using Mem-PER Membrane Protein Extraction Kit (Pierce) containing protease inhibitor mixture.

β-Hexosaminidase assays. Human fibroblasts were incubated with recombinant VEGF (10 ng ml^{-1}) and 2 mM mannose-6-phosphate at 37 °C. At the indicated time points, an aliquot of media was removed and assayed for β-hexosaminidase activity at 37 °C and pH 4.4 by using the synthetic substrate 4-methylumbelliferyl-*N*-acetyl-glucosaminide (Sigma-Aldrich). After the last time point, cells were lysed and an aliquot of the lysate assayed for β-hexosaminidase activity to determine the total enzyme activity of each sample. Enzyme activities were expressed as a percentage of the total enzyme activity found in the lysate. To confirm cell viability, LDH assays were performed, using an aliquot of culture medium taken at the indicated time points by an LDH assay kit (Sigma-Aldrich).

Cell viability. Viability of human iPSC-derived neurons was quantified by using WST-1 (Roche). Briefly, human iPSC-derived neurons were seeded on to 24-well plates at a density of 1×10^4 cells per well. Recombinant VEGF (10 ng ml^{-1}) was added to culture media, and the cells were incubated for an additional 72 h. WST-1 solution was then added to each well, and the cells were further incubated. After 4 h, the absorbance was measured with a plate reader at 440 nm.

Laser capture microscopy. LCM was performed by the P.A.L.M. Laser Pressure Catapult system (Zeiss Instruments) using standard procedures. Briefly, cerebella were immediately frozen into a block of tissue freezing medium (Electron Microscopy Sciences). The frozen blocks were cut into 8-µm-thick sections that were then mounted on Arcturus PEN membrane glass slides (Applied Biosystems). The slides were then stained with 0.1% crystal violet (Sigma-Aldrich) and viewed with a Zeiss Observer Z1 inverted light microscope using a ×40 objective. The Zeiss P.A.L.M. device uses a ultraviolet laser beam focused on a selected area of tissue. The collecting cap was placed over the targeted PNs, and by applying a single pulse of laser the targeted cells were catapulted into the collection cap. Total RNA from the isolated cells was extracted with the RNeasy Micro Kit (Qiagen) and then subjected to T7 RNA polymerase-based linear amplification using the Message BOOSTER kit for quantitative PCR (Epicentre).

Reverse-transcriptase PCR and quantitative real-time PCR. The RNeasy Lipid Tissue Mini kit or RNeasy Plus Mini Kit (Qiagen) was used for extraction of RNA from brain homogenates and cell lysates. Complementary DNA was synthesized from 5 µg of total RNA using the cDNA Synthesis Kit (Clontech) according to the manufacturer's protocol. Quantitative real-time PCR was performed using a Corbett research RG-6000 real-time PCR instrument. Used primers are described in Supplementary Table 1.

Behavioural studies. We performed behavioural studies to assess mouse balance and coordination by measuring the amount of time the animal was able to remain on a longitudinally rotating rod. Briefly, the Rota-rod apparatus (Ugo Basile) was set to an initial speed of 4 r.p.m., and the acceleration was increased by 32 r.p.m. every 25–30 s. Scores were registered every 3 days, and three independent tests were performed at each measurement.

Western blotting. Samples were lysed in RIPA buffer (Cell signaling Technologies), then subjected to SDS–PAGE and transferred to a nitrocellulose membrane. Membranes were blocked with 5% milk, incubated with primary antibody and then incubated with the appropriate horseradish peroxidase-conjugated secondary antibody. Primary antibodies to the following proteins were used: LC3 (rabbit, 1:1,000, 4108S) Beclin-1 (rabbit, 1:1,000, 3738S), p62 (rabbit, 1:1,000, 5114S), rab5 (rabbit, 1:1,000, 3547S), rab7 (rabbit, 1:1,000, 9367S), TFEB (rabbit, 1:1,000, 4240S; all from Cell Signaling Technologies), Lamp1 (rabbit, 1:1,000, Abcam, AB24170), TFEB (rabbit, 1:500, Novus, NBP1-67872), cathepsin D (goat, 1:500, R&D Systems, BAF1029) and β-actin (1:1,000, Santa Cruz, SC-1615). We carried out densitometric quantification using the ImageJ software (US National Institutes of Health). Full scans of western blots are provided in Supplementary Fig. 9.

Measurement of activity of cathepsin D. Enzyme activity of cathepsin D was determined with cathepsin D activity fluorometric assay kit according to the manufacturer's protocol (Abcam).

LysoTracker labelling and quantification. LysoTracker red (Invitrogen) was used at a final concentration of 75 nM. H_2O_2- and NH_4Cl-treated cells were used as positive and negative controls, respectively. The cells were trypsinized, resuspended in PBS and analysed on a FACS Calibur using FACSDiva software (Becton Dickinson).

Electron microscopy. Brain tissues and cells were fixed in 3% glutaraldehyde/0.1 M phosphate buffer, pH 7.4, and postfixed in 1% osmium tetroxide in Sorensen's phosphate buffer. After dehydration in ethyl alcohol, the tissues and cells were embedded in Epon (Electron Microscopy Sciences). Samples were cut serially and placed on copper grids and analysed using transmission electron microscope (Tecnai). Images were captured on a digital camera and Xplore3D tomography software.

Analysis of autophagic flux with mCherry-EGFP-LC3 reporter. mCherry-EGFP-LC3B (plasmid 22418) was acquired from Addgene. Transfection was performed using Lipofectamine2000 (Invitrogen) according to the manufacturer's protocol. Autophagososome and autolysosome were quantified by image J software.

Intracellular Ca^{2+} concentration. Changes in $[Ca^{2+}]_i$ were determined by a confocal laser scanning microscope using a C-apochromat ×40 objective (1.2 numerical aperture). The excitation wavelength for the detection of Ca^{2+} was 488 nm, and the emission wavelength was 516 nm. The fluorescent images were generated at 25 °C and analysed using LSM5 EXCITER software (Carl Zeiss). For the Ca^{2+} measurements, cells were loaded with the Ca^{2+}-sensitive dye fluo-4/acetoxymethyl ester (3 µmol l^{-1}; Molecular Probes, Eugene, OR, USA) in Krebs-Ringer phosphate-HEPES (KRPH) buffer containing 0.2% BSA (pH 7.4) for 30 min. The cells were incubated for 30 min in a dye-free solution to allow esterase cleavage of the fluo-4/acetoxymethyl ester to liberate fluo-4. After the establishment of a stable baseline $[Ca^{2+}]_i$ level, the cells were stimulated with 200 µM GPN for 5 min. GPN was applied using a flow system with a flow rate of ~1 ml min^{-1}. The images were collected at 5 s intervals, and the results were plotted as the change in fluorescence intensity expressed in arbitrary units. The magnitude was calculated as the change in fluorescence intensity expressed as a percentage of the basal fluorescence intensity (F_0). The area under the curve was calculated using Microcal Origin software version 7.0 (Northampton, MA, USA).

Lentiviral shRNA-mediated depletion of VEGF and NPC1. We cloned VEGF and NPC1 shRNAs into lentiviral vector plasmid CS-CDF-CG-PRE. The following short hairpin sequences were used: 5′-GATGTGAATGCAGACCAAAGA-3′ (SABiosciences-Qiagen; KM03041N; VEGF-shRNA #4); 5′-AGTTCCAG-TACGGCTCCAA-3′ (SABiosciences-Qiagen; KM03041N; NPC1-shRNA #3); and 5′-GGAATCTCATTCGATGCATAC-3′ (SABiosciences-Qiagen; negative control shRNA). The shRNA-expressing lentiviruses were produced by transient transfection of 293T cells[40]. Virus-containing media were collected, filtered and concentrated by ultracentrifugation at 50,000 *g* for 2 h and resuspended in PBS. Viral titres were measured by serial dilution on 293T cells, followed by flow cytometry analysis after 48 h. The titre of the virus used ranged between 2 and 5×10^9 plaque-forming units per ml. Three µl of lentiviruses was administered into the cerebellum of 4-week-old mice by stereotaxic injection 3 days before analysis as previously described[7].

Preparation of VEGF-loaded microspheres. VEGF-loaded poly(lactic-co-glycolic acid) (PLGA) microspheres were prepared using the method of water-in-oil-in-water emulsification[41]. Briefly, human recombinant VEGF-A (R&D Systems) in powder form was dispersed in PLGA (50:50 lactic to glycolic acid copolymer ratio

with a molecular weight of 40,000–75,000) solution in CH_2Cl_2 using a homogenizer. Polyvinylalcohol (PVA) solution (1%) was added to this mixture and homogenized. This emulsion was poured into a 0.1% PVA solution and stirred for 1 h. The hardened microspheres were centrifuged, filtered and washed and subsequently dried for 24 h under vacuum.

Maintenance and generation of iPSCs. Established iPSC and ES cells were maintained on mitomycin C-treated mouse embryonic fibroblasts (MEFs) in complete ES medium composed of DMEM (Sigma-Aldrich) supplemented with 20% knockout serum replacement, 5 ng ml^{-1} recombinant human basic fibroblast growth factor (FGF) (Peprotech), 20 mM HEPES buffer (pH 7.3), 0.1 mM 2-mercaptoethanol, 0.1 mM non-essential amino acids, 2 mM L-glutamine and 100 U ml^{-1} penicillin/streptomycin (all other materials were from Gibco). NP–C iPSCs were established from NP–C patient skin fibroblasts (GM03123, Coriell Institute)[42,43]. In brief, NP–C fibroblasts were seeded at 3×10^5 cells in 60-mm^2 dish coated with gelatin (Sigma-Aldrich). On day 1, the vesicular stomatitis virus G glycoprotein (VSV-G)-pseudotyped retroviral vector carrying *OCT4*, *SOX2*, *KLF4* and *c-MYC* was added to the fibroblasts. On day 2, cells were subjected to the same transduction procedures and harvested 24 h later. Transduced cells were replated on MEF layers in 100-mm^2 dish containing the fibroblast medium. On the next day, the medium was changed to complete ES medium with 0.5 mM valproic acid (Sigma-Aldrich), and thereafter changed every other day. After 20 days, ES-like colonies appeared and were picked up to be reseeded on new MEF layers. Cloned ES-like colonies were subjected to further analysis.

***In vitro* differentiation of human iPSCs.** Neural differentiation of iPSCs was performed[44]. Briefly, iPSC colonies were detached from feeder layers and cultured in suspension as embryoid body for about 30 days in bacteriological dishes. EBs were then enzymatically dissociated into single cells and the dissociated cells cultured in suspension in serum-free hormone mix media[44,45] for 10–14 days to allow the formation of neurospheres. Neurospheres were passaged repeatedly by dissociation into single cells, followed by culture in the same manner. Typically, neurospheres between passages 3 and 8 were used for analysis. For terminal differentiation, dissociated neurospheres were allowed to adhere to poly-L-ornithine- and laminin-coated coverslips and cultured for 10 days.

Alkaline phosphatase staining. Alkaline phosphatase staining was performed using an ES-alkaline phosphatase detection kit (Chemicon) according to manufacturer's recommendations.

Teratoma formation and histological analysis. Established iPSCs were prepared at 1×10^7 cells ml^{-1} in PBS. Suspended cells ($1–3 \times 10^6$) were injected into testes of anaesthetized male SCID Beige mice. Eight weeks after transplantation, mice were sacrificed and tumours were dissected. Tumor samples were fixed in 10% formalin and embedded in paraffin. Sections were stained with hematoxylin and eosin.

Statistical analysis. Comparisons between two groups were performed with Student's *t*-test. In cases where more than two groups were compared to each other, a one-way analysis of variance was used, followed by Tukey's honestly significant difference (HSD) test. Comparisons of overall survival were performed using a log-rank test. All statistical analysis was performed using SPSS statistical software. $P<0.05$ was considered to be significant.

References

1. Vanier, M. T. & Millat, G. Niemann-Pick disease type C. *Clin. Genet.* **64,** 269–281 (2003).
2. Vanier, M. T. Lipid changes in Niemann-Pick disease type C brain: personal experience and review of the literature. *Neurochem. Res.* **24,** 481–489 (1999).
3. Blom, T., Li, Z., Bittman, R., Somerharju, P. & Ikonen, E. Tracking sphingosine metabolism and transport in sphingolipidoses: NPC1 deficiency as a test case. *Traffic* **13,** 1234–1243 (2012).
4. Lloyd-Evans, E. *et al.* Niemann-Pick disease type C1 is a sphingosine storage disease that causes deregulation of lysosomal calcium. *Nat. Med.* **14,** 1247–1255 (2008).
5. Bae, J. S. *et al.* Bone marrow-derived mesenchymal stem cells promote neuronal networks with functional synaptic transmission after transplantation into mice with neurodegeneration. *Stem Cells* **25,** 1307–1316 (2007).
6. Bae, J. S. *et al.* Neurodegeneration augments the ability of bone marrow-derived mesenchymal stem cells to fuse with Purkinje neurons in Niemann-Pick type C mice. *Hum. Gene Ther.* **16,** 1006–1011 (2005).
7. Lee, H. *et al.* Bone marrow-derived mesenchymal stem cells prevent the loss of Niemann-Pick type C mouse Purkinje neurons by correcting sphingolipid metabolism and increasing sphingosine-1-phosphate. *Stem Cells* **28,** 821–831 (2010).
8. Le Stunff, H., Peterson, C., Liu, H., Milstien, S. & Spiegel, S. Sphingosine-1-phosphate and lipid phosphohydrolases. *Biochim. Biophys. Acta* **1582,** 8–17 (2002).
9. Shu, X., Wu, W., Mosteller, R. D. & Broek, D. Sphingosine kinase mediates vascular endothelial growth factor-induced activation of ras and mitogen-activated protein kinases. *Mol. Cell. Biol.* **22,** 7758–7768 (2002).
10. Xia, P. *et al.* Tumor necrosis factor-alpha induces adhesion molecule expression through the sphingosine kinase pathway. *Proc. Natl Acad. Sci. USA* **95,** 14196–14201 (1998).
11. Olivera, A. & Spiegel, S. Sphingosine-1-phosphate as second messenger in cell proliferation induced by PDGF and FCS mitogens. *Nature* **365,** 557–560 (1993).
12. Edsall, L. C., Pirianov, G. G. & Spiegel, S. Involvement of sphingosine 1-phosphate in nerve growth factor-mediated neuronal survival and differentiation. *J. Neurosci.* **17,** 6952–6960 (1997).
13. Spiegel, S. & Milstien, S. Sphingosine-1-phosphate: an enigmatic signalling lipid. *Nat. Rev. Mol. Cell Biol.* **4,** 397–407 (2003).
14. Wang, Y. *et al.* VEGF overexpression induces post-ischaemic neuroprotection, but facilitates haemodynamic steal phenomena. *Brain* **128,** 52–63 (2005).
15. Olsson, A. K., Dimberg, A., Kreuger, J. & Claesson-Welsh, L. VEGF receptor signalling - in control of vascular function. *Nat. Rev. Mol. Cell Biol.* **7,** 359–371 (2006).
16. Cvetanovic, M., Patel, J. M., Marti, H. H., Kini, A. R. & Opal, P. Vascular endothelial growth factor ameliorates the ataxic phenotype in a mouse model of spinocerebellar ataxia type 1. *Nat. Med.* **17,** 1445–1447 (2011).
17. Wood, J. M. *et al.* PTK787/ZK 222584, a novel and potent inhibitor of vascular endothelial growth factor receptor tyrosine kinases, impairs vascular endothelial growth factor-induced responses and tumor growth after oral administration. *Cancer Res.* **60,** 2178–2189 (2000).
18. Foraker, J. E. *et al.* Cross-talk between human mesenchymal stem/progenitor cells (MSCs) and rat hippocampal slices in LPS-stimulated cocultures: the MSCs are activated to secrete prostaglandin E2. *J. Neurochem.* **119,** 1052–1063 (2011).
19. Ruiz de Almodovar, C. *et al.* Matrix-binding vascular endothelial growth factor (VEGF) isoforms guide granule cell migration in the cerebellum via VEGF receptor Flk1. *J. Neurosci.* **30,** 15052–15066 (2010).
20. Sentilhes, L. *et al.* Vascular endothelial growth factor and its high-affinity receptor (VEGFR-2) are highly expressed in the human forebrain and cerebellum during development. *J. Neuropathol. Exp. Neurol.* **69,** 111–128 (2010).
21. Folkman, J. Angiogenesis in cancer, vascular, rheumatoid and other disease. *Nat. Med.* **1,** 27–31 (1995).
22. Ko, D. C. *et al.* Cell-autonomous death of cerebellar purkinje neurons with autophagy in Niemann-Pick type C disease. *PLoS Genet.* **1,** 81–95 (2005).
23. Rubinsztein, D. C. *et al.* In search of an 'autophagomometer'. *Autophagy* **5,** 585–589 (2009).
24. Settembre, C. *et al.* TFEB links autophagy to lysosomal biogenesis. *Science* **332,** 1429–1433 (2011).
25. Pankiv, S. *et al.* p62/SQSTM1 binds directly to Atg8/LC3 to facilitate degradation of ubiquitinated protein aggregates by autophagy. *J. Biol. Chem.* **282,** 24131–24145 (2007).
26. Bilmen, J. G., Khan, S. Z., Javed, M. H. & Michelangeli, F. Inhibition of the SERCA $Ca2^+$ pumps by curcumin. Curcumin putatively stabilizes the interaction between the nucleotide-binding and phosphorylation domains in the absence of ATP. *Eur. J. Biochem.* **268,** 6318–6327 (2001).
27. Chen, F. W., Li, C. & Ioannou, Y. A. Cyclodextrin induces calcium-dependent lysosomal exocytosis. *PLoS ONE* **5,** e15054 (2010).
28. Trilck, M. *et al.* Niemann-Pick type C1 patient-specific induced pluripotent stem cells display disease specific hallmarks. *Orphanet J. Rare Dis.* **8,** 144 (2013).
29. Maetzel, D. *et al.* Genetic and chemical correction of cholesterol accumulation and impaired autophagy in hepatic and neural cells derived from Niemann-Pick Type C patient-specific iPS cells. *Stem Cell Rep.* **2,** 866–880 (2014).
30. Yu, D. *et al.* Niemann-Pick disease type C: induced pluripotent stem cell-derived neuronal cells for modeling neural disease and evaluating drug efficacy. *J. Biomol. Screen.* **19,** 1164–1173 (2014).
31. Liscum, L. & Faust, J. R. Low density lipoprotein (LDL)-mediated suppression of cholesterol synthesis and LDL uptake is defective in Niemann-Pick type C fibroblasts. *J. Biol. Chem.* **262,** 17002–17008 (1987).
32. Griffin, L. D., Gong, W., Verot, L. & Mellon, S. H. Niemann-Pick type C disease involves disrupted neurosteroidogenesis and responds to allopregnanolone. *Nat. Med.* **10,** 704–711 (2004).
33. Meske, V., Erz, J., Priesnitz, T. & Ohm, T. G. The autophagic defect in Niemann-Pick disease type C neurons differs from somatic cells and reduces neuronal viability. *Neurobiol. Dis.* **64,** 88–97 (2014).
34. Liao, G. *et al.* Cholesterol accumulation is associated with lysosomal dysfunction and autophagic stress in $Npc1^{-/-}$ mouse brain. *Am. J. Pathol.* **171,** 962–975 (2007).

35. Panyam, J. & Labhasetwar, V. Biodegradable nanoparticles for drug and gene delivery to cells and tissue. *Adv. Drug Deliv. Rev.* **55,** 329–347 (2003).
36. Aebischer, P. & Ridet, J. Recombinant proteins for neurodegenerative diseases: the delivery issue. *Trends Neurosci.* **24,** 533–540 (2001).
37. Loftus, S. K. *et al.* Murine model of Niemann-Pick C disease: mutation in a cholesterol homeostasis gene. *Science* **277,** 232–235 (1997).
38. Takahashi, K. *et al.* Induction of pluripotent stem cells from adult human fibroblasts by defined factors. *Cell* **131,** 861–872 (2007).
39. Billich, A. & Ettmayer, P. Fluorescence-based assay of sphingosine kinases. *Anal. Biochem.* **324,** 114–119 (2004).
40. Miyoshi, H., Blomer, U., Takahashi, M., Gage, F. H. & Verma, I. M. Development of a self-inactivating lentivirus vector. *J. Virol.* **72,** 8150–8157 (1998).
41. Kim, T. K. & Burgess, D. J. Pharmacokinetic characterization of 14C-vascular endothelial growth factor controlled release microspheres using a rat model. *J. Pharm. Pharmacol.* **54,** 897–905 (2002).
42. Okita, K., Ichisaka, T. & Yamanaka, S. Generation of germline-competent induced pluripotent stem cells. *Nature* **448,** 313–317 (2007).
43. Okabe, M. *et al.* Definitive proof for direct reprogramming of hematopoietic cells to pluripotency. *Blood* **114,** 1764–1767 (2009).
44. Okada, Y. *et al.* Spatiotemporal recapitulation of central nervous system development by murine embryonic stem cell-derived neural stem/progenitor cells. *Stem Cells* **26,** 3086–3098 (2008).
45. Imaizumi, Y. *et al.* Mitochondrial dysfunction associated with increased oxidative stress and alpha-synuclein accumulation in PARK2 iPSC-derived neurons and postmortem brain tissue. *Mol. Brain* **5,** 35 (2012).

Acknowledgements

We thank Victor A. DeAngelis for help with UPLC analysis. We are grateful to Hyun Ok Kim and Tomoyuki Yamaguchi for kindly providing reagents. This work was supported by the Bio & Medical Technology Development Program (2011-0019356, 2012M3A9C6050107, 2012M3A9C6049913) of the National Research Foundation (NRF) of Korea funded by the Ministry of Science, ICT & Future Planning, Republic of Korea. This study was also supported by a grant of the Korea Healthcare Technology R&D Project, Ministry for Health & Welfare, Republic of Korea (A120367).

Author contributions

H.L., J.K.L., M.H.P., Y.R.H., H.K., Y.O., M.O., E.-J.S., J.-H.P., J.-H.B., N.O., X.H. and H.K.J. performed the experiments and analysed the data, J.-S.B. and H.K.J. designed the study and H.L., J.K.L. and J.-S.B. wrote the paper. E.H.S., J.-S.B. and H.K.J. interpreted the data and reviewed the paper. H.H.M. generated and provided $VEGF^{tg}$ mice. All authors discussed results and commented on the manuscript.

Additional information

Supplementary Information accompanies this paper at http://www.nature.com/naturecommunications

Competing financial interests: The authors declare no competing financial interest.

Reprints and permission information is available online at http://npg.nature.com/reprintsandpermissions/

How to cite this article: Lee, H. *et al.* Pathological roles of the VEGF/SphK pathway in Niemann–Pick type C neurons. *Nat. Commun.* 5:5514 doi: 10.1038/ncomms6514 (2014).

Archival Report

Biological Psychiatry

Utility of Scalp Hair Follicles as a Novel Source of Biomarker Genes for Psychiatric Illnesses

Motoko Maekawa, Kazuo Yamada, Manabu Toyoshima, Tetsuo Ohnishi, Yoshimi Iwayama, Chie Shimamoto, Tomoko Toyota, Yayoi Nozaki, Shabeesh Balan, Hideo Matsuzaki, Yasuhide Iwata, Katsuaki Suzuki, Mitsuhiro Miyashita, Mitsuru Kikuchi, Motoichiro Kato, Yohei Okada, Wado Akamatsu, Norio Mori, Yuji Owada, Masanari Itokawa, Hideyuki Okano, and Takeo Yoshikawa

ABSTRACT

BACKGROUND: Identifying beneficial surrogate genetic markers in psychiatric disorders is crucial but challenging.

METHODS: Given that scalp hair follicles are easily accessible and, like the brain, are derived from the ectoderm, expressions of messenger RNA (mRNA) and microRNA in the organ were examined between schizophrenia (*n* for first/second = 52/42) and control subjects (*n* = 62/55) in two sets of cohort. Genes of significance were also analyzed using postmortem brains (*n* for case/control = 35/35 in Brodmann area 46, 20/20 in cornu ammonis 1) and induced pluripotent stem cells (*n* = 4/4) and pluripotent stem cell-derived neurospheres (*n* = 12/12) to see their role in the central nervous system. Expression levels of mRNA for autism (*n* for case/control = 18/24) were also examined using scalp hair follicles.

RESULTS: Among mRNA examined, *FABP4* was downregulated in schizophrenia subjects by two independent sample sets. Receiver operating characteristic curve analysis determined that the sensitivity and specificity were 71.8% and 66.7%, respectively. *FABP4* was expressed from the stage of neurosphere. Additionally, microarray-based microRNA analysis showed a trend of increased expression of *hsa-miR-4449* ($p = .0634$) in hair follicles from schizophrenia. *hsa-miR-4449* expression was increased in Brodmann area 46 from schizophrenia ($p = .0007$). Finally, we tested the expression of nine putative autism candidate genes in hair follicles and found decreased *CNTNAP2* expression in the autism cohort.

CONCLUSIONS: Scalp hair follicles could be a beneficial genetic biomarker resource for brain diseases, and further studies of *FABP4* are merited in schizophrenia pathogenesis.

Keywords: Autism, *CNTNAP2*, FABP4, *hsa-miR-4449*, MicroRNA, Schizophrenia

http://dx.doi.org/10.1016/j.biopsych.2014.07.025

The disease mechanisms underlying psychiatric illnesses remain largely undetermined. Great efforts have gone into identifying novel biomarkers that would assist in the development of objective diagnostic tools and novel therapeutic and prophylactic interventions, as well as facilitate the subdivision of disease states, based on pathogenesis, for optimal drug selection. There are, however, major obstacles in the search for novel biomarkers, primarily the difficulty in obtaining brain tissue from living donors and the lack of accurate experimental animal models. Brain is an ectodermal tissue and shares its developmental origins with scalp hair follicles, which are readily accessible miniorgans within the skin. Despite their shared embryonic origins, hair follicles have not previously been utilized as a bio-resource in the hunt for proxy genes in psychiatric diseases. In the current study, we first examined whether schizophrenia-relevant genes, namely those related to the γ-aminobutyric acid (GABA)ergic system (1–3), myelin (3–5), and fatty acids (6–11), are expressed in hair follicles and if expressed whether expression is differential between cases and control subjects, using an exploratory sample set. Next, we attempted to validate any differential expression and examine the effects of potential confounding factors using a second independent sample set. We then analyzed the identified biomarker candidate *FABP4*/fatty acid binding protein 4 (FABP4) expression in serum, postmortem brain samples, induced pluripotent stem cells (iPSCs), and iPSC-derived neurospheres. In addition to messenger RNA (mRNA), we also examined the expression levels of microRNA (miRNA) in hair follicles, postmortem brains, iPSCs, and iPSC-derived neurosphere samples from patients with schizophrenia and control subjects. Lastly, we tested candidate gene expression in hair follicles from patients with autism. Based on the results of our comprehensive analysis, we proposed scalp hair follicles as a beneficial genetic resource for schizophrenia and autism in the search for potential biomarkers.

ISSN: 0006-3223

Biological Psychiatry ▮▮▮, 2014; ▮:▮▮▮–▮▮▮ www.sobp.org/journal

METHODS AND MATERIALS

Scalp Hair Follicle Samples

All samples were collected from ethnic Japanese within Japan. The first set of exploratory scalp hair follicle samples for schizophrenia and control subjects was derived from residents in the northern district of Kanto, while the confirmatory second set came from the Tokyo area. Diagnoses were made by at least two experienced psychiatrists, using DSM-IV criteria. Demographic data for scalp hair follicle samples derived from schizophrenia are described in Table 1. The scalp hair follicle samples from autism participants and control subjects were collected from the Chubu area. The diagnosis of autism spectrum disorder was made using the DSM-IV-TR criteria. We then administered the Autism Diagnostic Interview-Revised (ADI-R) (12) to 14 of 18 cases and made a confirmed diagnosis of autism for those 14 cases. Interviews for the ADI-R were conducted by experienced child psychiatrists who are licensed to use the Japanese version of the ADI-R (13). Demographic data relating to scalp hair follicle samples for autism are described in Table 1.

RNA Extraction and Quantification

Ten hairs were plucked from the scalp of each subject using forceps. The hairs were checked for the presence of a sheath. Hairs were trimmed to approximately 1.5 cm in length, containing the bulb region, and dropped into a 1.5 mL microfuge tube (BM Equipment, Tokyo, Japan) containing RNAlater solution (Ambion, Grand Island, New York). Total RNA was extracted using the RNAqueous-Micro kit (Ambion). Single-stranded complementary DNA (cDNA) was synthesized using SuperScript VILO Master Mix (Invitrogen, Grand Island, New York). Quantitative reverse-transcription PCR (qRT-PCR) analysis of mRNAs was conducted using an ABI7900HT Fast Real-Time PCR System (Applied Biosystems, Grand Island, New York). TaqMan probes were TaqMan Gene Expression Assays products (Applied Biosystems). All qRT-PCR data were captured using the SDS v2.4 (Applied Biosystems). The ratios of relative concentrations of target molecules to the *GAPDH* gene (target molecule/*GAPDH* gene) were calculated. All reactions were performed in triplicate based on the standard curve method.

Statistical Analysis

We used the interquartile range to find outliers. The differences between the 25th (quartile 1) and 75th percentiles (quartile 3) were used to identify extreme values (outliers) in the tails of the distribution. Statistical evaluation was performed by Mann-Whitney *U* test for means between patient and control groups and by Spearman's R test for correlation using SPSS software version 19 (IBM, Tokyo, Japan).

Analyses of miRNA Expressions and Potential Targets of miRNAs

For microarray-based miRNA analysis, we used the miRBase Rel. 18.0 platform (Agilent Technologies, Santa Clara California), capable of measuring 1919 human mature miRNAs in the age-/sex-matched subset of the first hair follicle sample set (Table S1 in Supplement 1). The miRNAs were labeled using the miRNA Complete Labeling Reagent and Hyb Kit (Agilent Technologies) and hybridized to the arrays. Images were scanned with a High-Resolution C scanner (Agilent Technologies) and analyzed using GeneSpring GX (Agilent Technologies). Comparisons of miRNA expression values between schizophrenia and control groups were performed using GeneSpring 12.6 (Agilent Technologies). To normalize the intermicroarray range of expression intensities, the percentile shift method (90th percentile) was used. The genes whose expression data were available in more than 50% of hybridizations were statistically evaluated between schizophrenia and control groups using the two-tailed Mann-Whitney *U* test. For quantification of individual miRNAs, we performed TaqMan-based miRNA qRT-PCR (Applied Biosystems, Grand Island, New York) according to the manufacturer's instructions, using *U6 snRNA* as a control probe. All reactions for miRNA quantification were also performed in triplicate, based on the standard curve method. Statistical evaluation methods were the same as those for mRNA.

Table 1. Demographic Characteristics of Hair Follicle Sample Sets

	Control Subjects	Patients	*p* Value
First Sample Set for Schizophrenia			
n	62	52	
Sex (female/male)	41 / 21	25 / 27	.0518[a]
Age (mean ± SD)	41.26 ± 12.26	50.98 ± 10.86	<.0001[b]
Second Sample Set for Schizophrenia			
n	55	42	
Sex (female/male)	26 / 29	20 / 22	.973[a]
Age (mean ± SD)	46.87 ± 13.56	49.93 ± 12.97	.2777[b]
Duration of illness (mean ± SD)		22.79 ± 14.66	
Autism Sample Set			
n	24	18	
Sex (female/male)	24 / 0	16 / 2	.1777[a]
Age (mean ± SD)	32.60 ± 3.91	25.61 ± 4.95	<.0001[b]

[a]Evaluated by chi-square test.
[b]Evaluated by two-tailed *t* test.